


Article

# Enhanced Selective Hydrogen Permeation through Graphdiyne Membrane: A Theoretical Study

Quan Liu <sup>1,\*</sup> , Long Cheng <sup>2</sup> and Gongping Liu <sup>2,\*</sup> <sup>1</sup> Analytical and Testing Center, Anhui University of Science and Technology, Huainan 232001, China<sup>2</sup> State Key Laboratory of Materials-Oriented Chemical Engineering, College of Chemical Engineering, Nanjing Tech University, 30 Puzhu Road (S), Nanjing 211816, China; longcheng@njtech.edu.cn

\* Correspondence: quanliu@aust.edu.cn (Q.L.); gpliu@njtech.edu.cn (G.L.)

Received: 29 September 2020; Accepted: 13 October 2020; Published: 15 October 2020



**Abstract:** Graphdiyne (GDY), with uniform pores and atomic thickness, is attracting widespread attention for application in H<sub>2</sub> separation in recent years. However, the challenge lies in the rational design of GDYs for fast and selective H<sub>2</sub> permeation. By MD and DFT calculations, several flexible GDYs were constructed to investigate the permeation properties of four pure gas (H<sub>2</sub>, N<sub>2</sub>, CO<sub>2</sub>, and CH<sub>4</sub>) and three equimolar binary mixtures (H<sub>2</sub>/N<sub>2</sub>, H<sub>2</sub>/CO<sub>2</sub>, and H<sub>2</sub>/CH<sub>4</sub>) in this study. When the pore size is smaller than 2.1 Å, the GDYs acted as an exceptional filter for H<sub>2</sub> with an approximately infinite H<sub>2</sub> selectivity. Beyond the size-sieving effect, in the separation process of binary mixtures, the blocking effect arising from the strong gas–membrane interaction was proven to greatly impede H<sub>2</sub> permeation. After understanding the mechanism, the H<sub>2</sub> permeance of the mixtures of H<sub>2</sub>/CO<sub>2</sub> was further increased to 2.84 × 10<sup>5</sup> GPU by reducing the blocking effect with the addition of a tiny amount of surface charges, without sacrificing the selectivity. This theoretical study provides an additional atomic understanding of H<sub>2</sub> permeation crossing GDYs, indicating that the GDY membrane could be a potential candidate for H<sub>2</sub> purification.

**Keywords:** graphdiyne; molecular simulation; membrane separation; hydrogen purification

## 1. Introduction

As an attractive alternative fuel source, hydrogen (H<sub>2</sub>) could eliminate the use of polluting fossil fuels in industry and transport in the future [1]. So, the H<sub>2</sub> energy is critical to reduce global greenhouse gases and promote sustainable development because of its natural abundance and high efficiency of combustion [2,3]. Today, in many industrial and drilling streams, H<sub>2</sub> is mainly produced from natural gas, hydro-electrolysis, and the combustion of hydrides [4,5]. However, these processes release several million tonnes of by-products (such as carbon dioxide, nitrogen, and methane) per year [6]. How to separate the target product of H<sub>2</sub> from the undesirable species is crucial to improve production efficiency and reduce the cost. Traditional separation techniques, such as pressure swing adsorption and cryogenic separation, would consume a considerable amount of energy to collect H<sub>2</sub> [7]. With the improved performances and lower operating conditions, the advanced membrane-based separation is seen as an alternative to significantly improve energy efficiency [8,9]. At room temperature and low transmembrane pressure, it is more instructive for experiments to develop membranes with both good H<sub>2</sub> permeance and selectivity. [10].

Recently, two-dimensional (2D) carbon-based membranes have sparked global attention due to their atomic thickness [11]. Among various membranes, graphene-based materials are, assuredly, one of the powerful candidates for membrane separation according to our previous experimental [12,13] and simulation studies [14,15]. According to the separation mechanism of the size sieving effect, controllable pores in the 2D-material membrane are imperative for gas separation. However, it is

not cost-effective to drill uniform pores in graphene, and this process may introduce non-selective defects in the membrane [16]. Alternatively, newly emerged graphdiyne (GDY) allotropes that formed by the periodic combination of sp and sp<sup>2</sup> carbon atoms are proposed as alternative options for gas purification [16], because they possess the well-distributed pores as well as the atomic membrane thickness [17]. Several studies have been reported to explore the gas permeation property through GDYs in recent years [18–20]. It is the comparable pores in GDYs that contribute to the outstanding gas separation properties, as Smith et al. first reported that the excellent H<sub>2</sub> separation performance was ascribed to the small triangular pores in the GDYs [21]. This later reports also showed that the various sized pores in diverse GDYs could be employed to distinguish the different sized molecules, such as He [18], O<sub>2</sub> [22], and CO<sub>2</sub> [23,24], concluding that the size sieving effect dominated the transport mechanism of GDYs for gas separation.

Although the pore size is an important factor for gas separation membranes, other factors, particularly the surface properties, should not be neglected. Sang et al. [25] and Smith et al. [26] found that the functionalized surface of GDYs shown a better separation performance than that of the pristine one. Moreover, the adsorption phenomenon in GDYs also affected the permeation of gases, such as H<sub>2</sub>S [27] and CO<sub>2</sub> [24,28]. It means, beyond the well-understood size sieving effect, there could be a more comprehensive mechanism to better describe gas transport through GDYs [19]. However, the main challenge is how such a mechanism determines the gas permeation properties, especially for selective H<sub>2</sub> permeation through GDYs, and how it contributes to further improvement of the H<sub>2</sub> permeance and selectivity of GDYs. In addition, most previous works focused on the first-principles calculations density functional theory (DFT) to study the selectivity of H<sub>2</sub> over CO<sub>2</sub>, CO, N<sub>2</sub>, and CH<sub>4</sub> [25,26,29]. A few studies calculated the H<sub>2</sub> permeance by performing molecular dynamic (MD) simulations, which however were based on a rigid framework of GDYs [20,23,30] and might be too idealized for actual GDYs for gas separation. Moreover, it is unclear what the ultimate size of nanopores in GDYs is allowed to transport H<sub>2</sub> molecules. Therefore, it is necessary to further understand the underlying separation mechanism of H<sub>2</sub> purification through a carefully designed flexible GDY membrane that possesses both high H<sub>2</sub> permeance and selectivity and find the ultimate diameter in GDYs for H<sub>2</sub> permeation.

In this work, a series of 2D GDYs are computationally constructed to examine the permeation of four pure gases (H<sub>2</sub>, N<sub>2</sub>, CO<sub>2</sub> and CH<sub>4</sub>) and their equimolar binary mixtures (H<sub>2</sub>/N<sub>2</sub>, H<sub>2</sub>/CO<sub>2</sub> and H<sub>2</sub>/CH<sub>4</sub>). Assuming that the separation performance of H<sub>2</sub> is affected by pore structures and surface charges, we systematically investigated these two effects by both MD and DFT calculations. Following the introduction, the atomic models of GDYs, as well as the separation systems, are illustrated in Section 2. In Section 3, the H<sub>2</sub> permeance is calculated by the time evolution of the permeated molecules according to the MD results, and the ideal selectivity is evaluated by DFT calculations. This separation mechanism of H<sub>2</sub> from binary mixtures is revealed by analyzing the diffusion coefficient, density contour, and energy barrier of the permeation. After that, the H<sub>2</sub> permeance of the mixture of H<sub>2</sub>/CO<sub>2</sub> is further improved by reducing the blocking effect. Finally, the concluding remarks are summarized in Section 4.

## 2. Models and Methods

The GDYs were constructed in the Material studio [31] and then subjected to geometry optimization in the Forcite module with 5000 iterations. As presented in Figure 1a–d, the dimensions of the membranes were 7.75 × 7.55 nm<sup>2</sup> in this setup, and the investigated pore diameters were varied from 1.5 to 2.5 Å, which were measured according to the formula:  $D = 2\sqrt{A/\pi}$  by inserting a van der Waals sphere, where  $A$  is the open pore area, as depicted in Figure 1e–h. We noted that the membrane in Figure 1b coded as GDY\_1.5Å\_p7% has the porosity of 7%, which is larger than that of 3% in Figure 1a (GDY\_1.5Å\_p3%), although both of these two membranes have a similar pore diameter of 1.5 Å. This above-mentioned porosity was calculated by the formula  $p = \frac{A_{pore}}{A_{mem}}$ , where  $A_{pore}$  and  $A_{mem}$  denote to the areas of the totally unoccupied regions and the membrane surface, respectively.

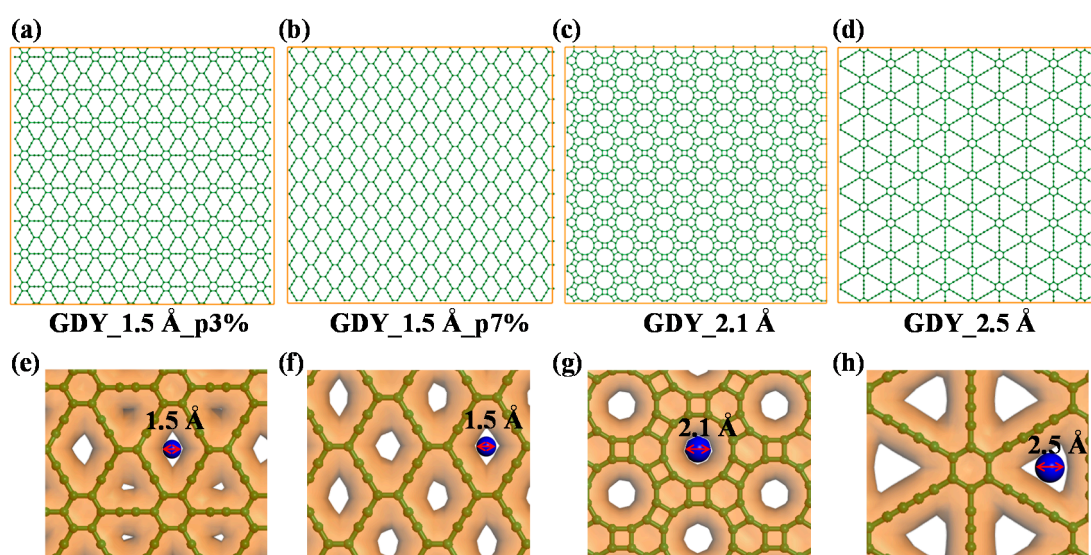


**Figure 1.** Membrane models. Atomic structures of graphdiyne (GDY) membranes with different pore structures: (a) GDY\_1.5Å\_p3%; (b) GDY\_1.5Å\_p7%; (c) GDY\_2.1Å; and (d) GDY\_2.5Å. This first two membranes have different porosities of 3% and 7%, respectively. (e–h) The criterion for the definition of the pore diameter in each GDY membranes.

Based on the optimized membranes, MD calculations were performed to simulate the gas separation. Figure 2 shows the simulation system, where two chambers were isolated by the GDY membrane. This left chamber was a gas reservoir, comprising 2000 molecules of pure gases (or binary mixtures with the mixing ratio of 1000:1000, in volume ratio). This right one treated as a vacuum is the permeate side, which is the most common setting in MD simulations for collecting the permeated molecules. [20,23,30] At both ends of each chamber, rigid graphene was placed to prevent molecules from roaming between the periodic boxes. Considering that carbon-based membranes usually have good flexibility in experiments [32], all pores in GDYs were treated as flexible in our present work so that the atoms around pores could perform small displacements. Thus, the aperture would be enlarged to allow the passage of H<sub>2</sub> even though the molecular size is larger than the pore size. On the contrary, the atoms on the edge of membranes were imposed with a position restriction to ensure the uniform lattice of GDYs and decrease the impact on gas permeation [33]. Furthermore, no collapse appeared in our system, suggesting good stability of the flexible structures. This framework of GDYs was described by the all-atom optimized potential. This four gases were represented by Lennard–Jones (LJ) and electrostatic potentials originating from our previous work [14]. Between dissimilar atoms, the interactions were assembled by the Lorentz–Berthelot combination rule [34].

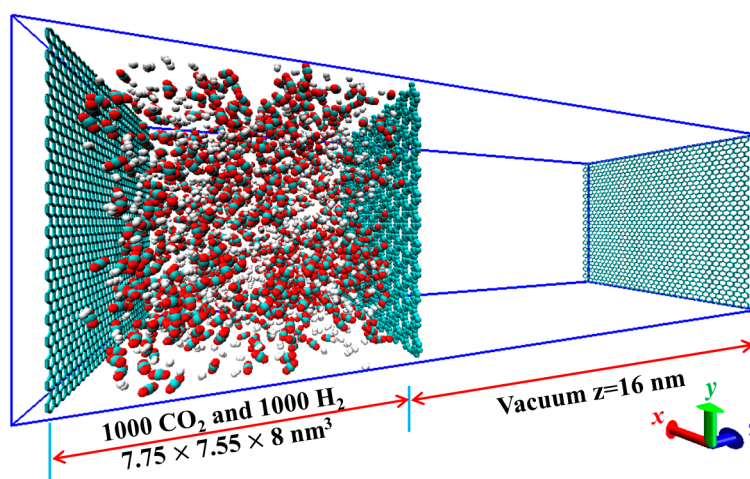


**Figure 2.** Simulation system of the equimolar binary mixture of H<sub>2</sub>/CO<sub>2</sub> permeating through the GDY\_2.1Å membrane. Atom: C (Cyan); O (red); H (white).

In this study, MD simulations were all carried out using the GROMACS package (version 4.5.5) [35]. A static minimization with the steepest descent method was first carried out to remove the unreasonable contacts among each atom. Then, the separation system was pre-equilibrated in the isobaric–isothermal ensemble (constant temperature and constant pressure ensemble, named as NPT) for 2 ns only in the z-direction. Following this, another 20 ns MD simulations were performed in the canonical ensemble (constant temperature and constant volume ensemble, named as NVT) for data collection and further analysis, and the trajectories were stored every 1 ps. During the simulations, the classical equations of motion were integrated with a time step of 1 fs by using the leapfrog algorithm. This temperature was maintained at 300 K by coupling with the velocity rescaling [36] thermostats. This long-range electrostatic interactions were computed by using the method of particle mesh Ewald [37]. While the short-range van der Waals interactions were truncated at a cut-off distance of 1.2 nm, the periodic boundary conditions were implemented in all three directions. With the partial pressure gradient as the driving force [38], the gases would permeate through the GDYs. For a better understanding of the separation process, an animation is provided in the Supplementary Materials (Video S1).

### 3. Results and Discussion

#### 3.1. Gas Permeation Behavior

The relationship between gas flux ( $J$ , mol·m<sup>-2</sup>·s<sup>-1</sup>) and permeance ( $S$ , mol·m<sup>-2</sup>·s<sup>-1</sup>·Pa<sup>-1</sup>) was described as Equation (1):

$$J = \frac{dN}{A_{mem}N_A dt} = \Delta P S \tag{1}$$

where  $N$  refers to the number of permeated molecules,  $N_A$  is the Avogadro constant, and  $\Delta P$  is the transmembrane gas partial pressure estimated by Equation (2):

$$\Delta P = \frac{(N_0 - N_{ad} - N)kT}{V_l} - \frac{NkT}{V_r} \tag{2}$$

in which  $N_{ad}$  refers to the number of gases adsorbed on the membrane surface,  $V_l$  and  $V_r$  are the volumes of the left and right chambers, respectively, and  $k$  represents the Boltzmann constant. Therefore, the time evolution of the number of permeated molecules is integrated as Equation (3), where  $R$  is the gas constant,

$$N = \frac{(N_0 - N_{ad})L_r}{(L_l + L_r)} \left( 1 - e^{-\frac{RTS(L_l + L_r)}{L_l L_r} t} \right) = \frac{2(N_0 - N_{ad})}{3} (1 - e^{-467.7St}). \tag{3}$$

As presented in Figure 3a, the number of permeated H<sub>2</sub> is increased exponentially with the simulation time, which agrees well with the above mathematical analysis. This permeance of pure H<sub>2</sub> is shown in Figure 3b. Obviously, it is remarkably enhanced with the increase of porosity and pore size. With the smallest pore of 1.5 Å, the porosity of 0.03 and 0.07 have the H<sub>2</sub> permeance of  $1.34 \times 10^5$  and  $2.55 \times 10^5$  GPU (1 GPU =  $3.35 \times 10^{-10}$  mol·m<sup>-2</sup>·s<sup>-1</sup>·Pa<sup>-1</sup>), respectively. This permeation of other gases (i.e., CO<sub>2</sub>, N<sub>2</sub> and CH<sub>4</sub>) through the GDYs was also simulated. It was shown that only the biggest pore with 2.5 Å allowed the passage of N<sub>2</sub>, CO<sub>2</sub>, and CH<sub>4</sub>, as presented in Figure 3c. This incompatibility of the kinetic diameter of gases (i.e., H<sub>2</sub>, 2.89 Å; N<sub>2</sub>, 3.64 Å; CO<sub>2</sub>, 3.30 Å; CH<sub>4</sub>, 3.8 Å) [39], and the pore size is ascribed to the flexible structures, implying that the membrane of GDY\_2.5Å is not suitable for H<sub>2</sub> purification. Moreover, the comparable pore with 2.1 Å diameter can not only completely block the other three gases but also process the good H<sub>2</sub> permeance of  $5.94 \times 10^5$  GPU, which implies that the selectivities of H<sub>2</sub> over CO<sub>2</sub>, N<sub>2</sub>, and CH<sub>4</sub> can be extremely high in the membrane of GDY\_2.1Å. We noted that the molecules of N<sub>2</sub>, CO<sub>2</sub>, and CH<sub>4</sub> can not be detected in the permeation side as long as the pore diameter was smaller than 2.1 Å, indicating the infinitely low permeance of N<sub>2</sub>, CO<sub>2</sub>, and CH<sub>4</sub>.

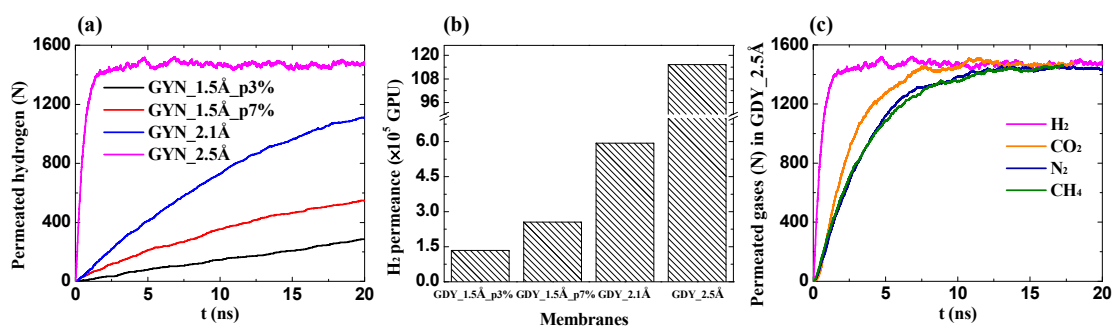


**Figure 3.** Pure gas permeation. (a) The time evolution of permeated H<sub>2</sub> molecules; (b) The permeance of H<sub>2</sub> through different GDYs; (c) The permeation of four gases in GDY\_2.5Å.

To evaluate the ideal selectivities of H<sub>2</sub> over other three gases in GDY\_2.1 Å, the DFT calculations were performed to calculate permeation barriers as per our previous study [15]. Figure 4a illustrates the minimum energy pathway (MEP) of four gases crossing the membrane. This inset configurations are the energetically stable states of CO<sub>2</sub> permeation at different locations. By searching the saddle point in MEPs, the energy barriers of permeation can be calculated. Evidently, the permeation barrier of H<sub>2</sub> crossing the flexible GDY\_2.1 Å is drastically reduced to 1.55 kJ/mol (Figure 4a, inset), which results in extraordinary H<sub>2</sub> permeance. On the contrary, the permeation barriers of CO<sub>2</sub>, N<sub>2</sub>, and CH<sub>4</sub> are all extremely high. In Figure 4b, the temperature-dependent H<sub>2</sub> selectivity has an inverse correlation with the temperature according to the Arrhenius Equation (4), whereas  $P_i$  is the permeation rate,  $A$  is the permeation prefactor that can be assumed as  $10^{11}$  s<sup>-1</sup> [38], and  $T$  is the temperature. For H<sub>2</sub>/CO<sub>2</sub> and H<sub>2</sub>/N<sub>2</sub>, the ideal selectivities of H<sub>2</sub> can be up to  $10^{17}$  at 300 K, which is the same order with the modified GDYs [25]. It remains very high ( $>10^8$ ) even at 600 K, further suggesting the extraordinary H<sub>2</sub> separation performance through GDY\_2.1 Å.

$$S_{i/j} = \frac{P_i}{P_j} = \frac{A_i \exp\left(-\frac{E_{\text{barrier}, i}}{RT}\right)}{A_j \exp\left(-\frac{E_{\text{barrier}, j}}{RT}\right)} \quad (4)$$

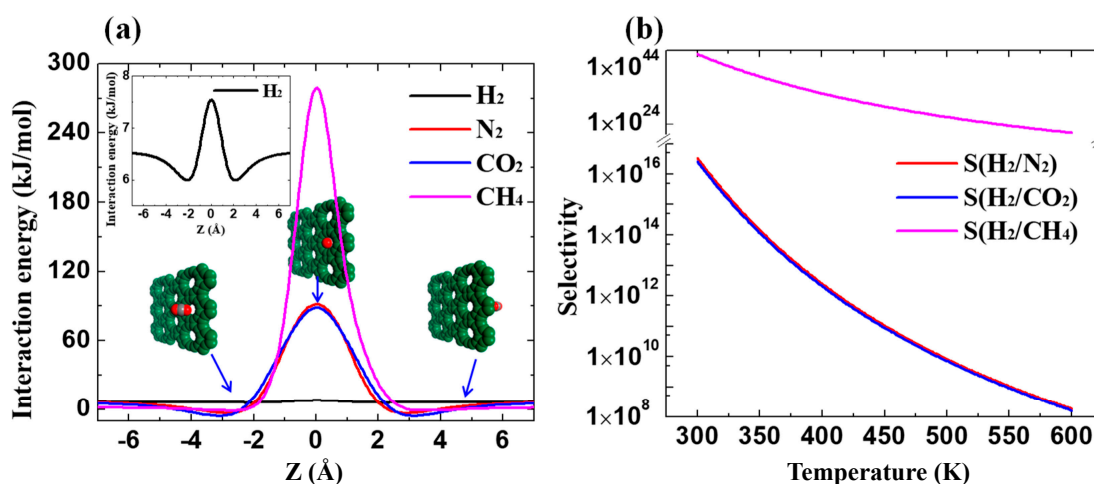


**Figure 4.** DFT calculations of gases crossing the membrane of GDY\_2.1Å. (a) Minimum energy pathways of four gases. (b) Ideal selectivities of H<sub>2</sub> over N<sub>2</sub>, CO<sub>2</sub>, and CH<sub>4</sub> as functions of temperature.

### 3.2. Transport Mechanism: Blocking Effect

For binary gas mixtures, the MD calculations were also performed to simulate the separation process. To visualize H<sub>2</sub> purification properties through the membrane of GDY\_2.1Å, the equilibrium configurations of final frames are presented in Figure 5a–c. As seen, the GDY\_2.1Å membrane acts as an effective filter for H<sub>2</sub> separation while completely blocking the passage of CO<sub>2</sub>, N<sub>2</sub>, and CH<sub>4</sub>, so that the H<sub>2</sub> is largely gathering in the vacuum chamber. This corresponding H<sub>2</sub> permeance of the three binary mixtures is presented in Figure 5d. Interestingly, the mixture of H<sub>2</sub>/N<sub>2</sub> exhibits the highest H<sub>2</sub> permeance of  $4.71 \times 10^5$  GPU, which is a little higher than that of H<sub>2</sub>/CH<sub>4</sub> and almost twice as many as the mixture of H<sub>2</sub>/CO<sub>2</sub>. This primary reason is that on the membrane surface, the strongly interacting gas (CO<sub>2</sub>) preferentially adsorbs, blocking the transport pores of H<sub>2</sub> molecules, thus resulting in a relatively low H<sub>2</sub> permeance.

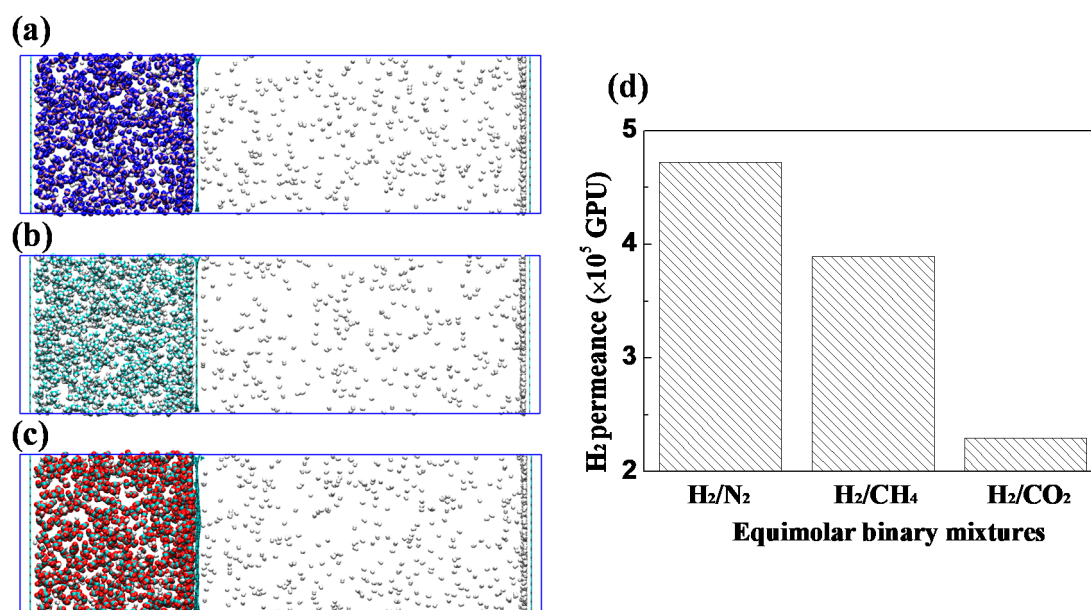


**Figure 5.** H<sub>2</sub> permeation of three equimolar binary mixtures crossing the GDY\_2.1Å. This final snapshots: (a) H<sub>2</sub>/N<sub>2</sub>, (b) H<sub>2</sub>/CH<sub>4</sub>, and (c) H<sub>2</sub>/CO<sub>2</sub>. Blue: N; cyan: C; red: O; white: H. (d) The H<sub>2</sub> permeance of different binary mixtures.

Further analyses are carried out to understand this blocking effect. This radial distribution function (RDF) was calculated to present the affinity of GDY\_2.1Å to four gases by using Equation (5):

$$g_{ij}(r) = \frac{N_{ij}(r, r + \Delta r)V}{4\pi r^2 \Delta r N_i N_j} \tag{5}$$

where  $N_{ij}(r, r + \Delta r)$  is the number of species  $j$  around  $i$  within a shell from  $r$  to  $r + \Delta r$ ,  $r$  is the distance between two species, and  $N_i$  and  $N_j$  refer to the numbers of atom types  $i$  and  $j$ , respectively. As presented in Figure 6a, there is an increasing trend of the gas–membrane interaction as  $H_2 < N_2 < CH_4 < CO_2$ . This weakest interaction together with the smallest molecular size endows  $H_2$  with exceptional permeance. Meanwhile, the strong interaction promotes the gases, particularly  $CO_2$  to preferentially adsorb on the membrane surface. To offer more intuitionistic information, the density contours of the distribution of  $N_2$ ,  $CH_4$ , and  $CO_2$  were plotted on the GDY\_2.1Å surface. This general distribution behavior of the three gases is similar as shown in Figure 6b–d, where the pores that are largely clogged by these gases are larger than the pore diameters. Nevertheless, the intensity of gas accumulation is quite different. As seen in Figure 6d, the pores are the most clogged, with the number of adsorbed  $CO_2$  molecules exceeding  $6.5 N_w/uc$  in every pore. Similar to the affinity analysis in Figure 6a, the extent of the blocking effect follows the increasing trend of  $N_2 < CH_4 < CO_2$ , decreasing the placeholders of  $H_2$  on the membrane surface in Figure 7a.

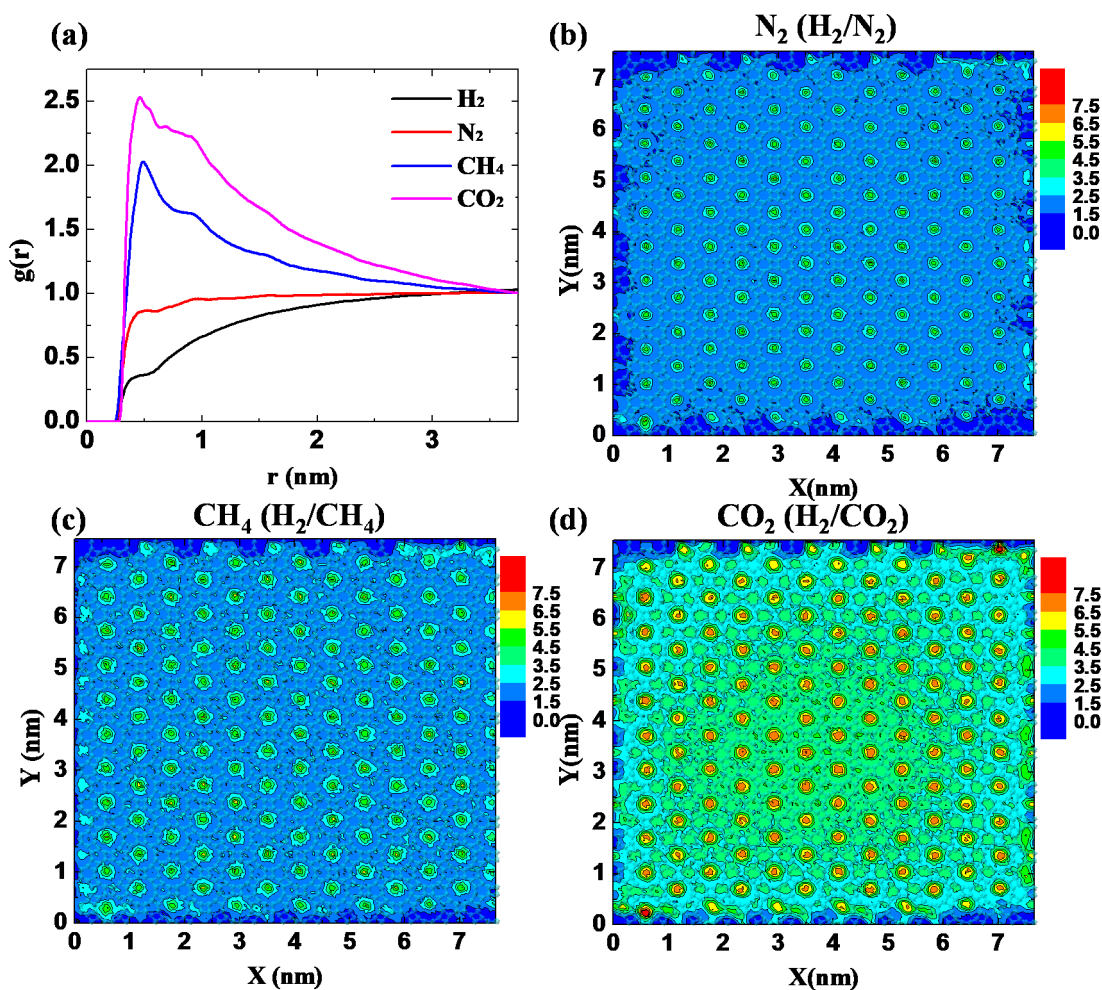


**Figure 6.** Blocking effect on the surface of GDY\_2.1Å. (a) Radial distribution function (RDF) of gases around the membrane. Density contours of the impermeable gases on the surface: (b)  $N_2 (H_2/N_2)$ ; (c)  $CH_4 (H_2/CH_4)$ ; (d)  $CO_2 (H_2/CO_2)$ . This unit of density ( $N_w/uc$ ) is  $1/(1.25\text{Å}^3)$ .

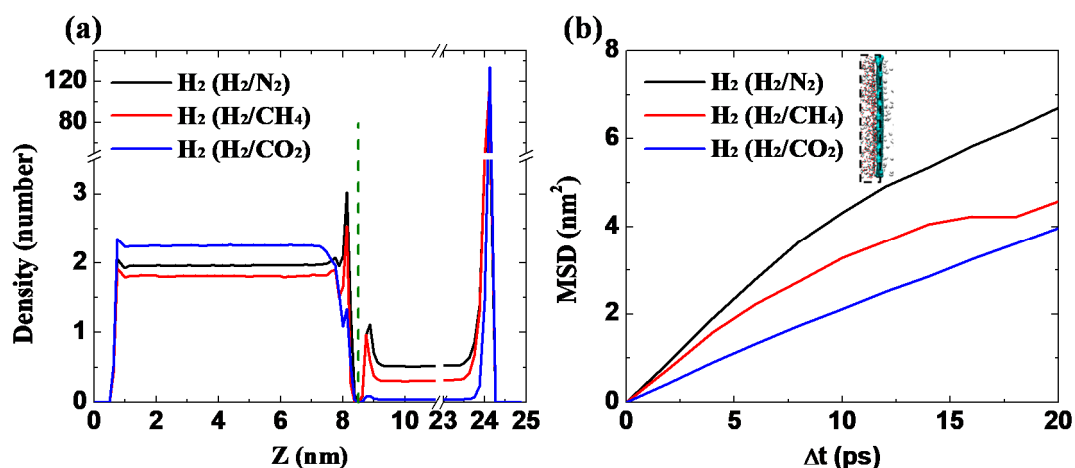


**Figure 7.** Permeation behavior of H<sub>2</sub> in binary mixtures. (a) The number distributions along the z-direction in the last 10 ns. This membrane is located at the green dotted line; (b) The mean square displacement (MSD) curves of H<sub>2</sub> crossing the GDY\_2.1Å membrane. (Inset) The region within 0.5 nm of the membrane surface for MSD calculation.

According to the first peak in Figure 6a, the mean square displacement (MSD) of H<sub>2</sub> molecules was analyzed within 0.5 nm of the membrane surface (Figure 7b, inset) from

$$MSD(t) = \frac{1}{N} \left\langle \sum_{i=1}^N (r_i(t)^2 - r_i(t_0)^2) \right\rangle \quad (6)$$

$$D = \frac{1}{6} \lim_{t \rightarrow \infty} \frac{dMSD(t)}{dt} \quad (7)$$

where  $r_i(t)^2 - r_i(t_0)^2$  refers to the distance traveled by the atom ( $i$ ) over the time interval of  $t - t_0$ . This diffusion coefficient ( $D$ ) is determined by the linear slope of the MSD curve with Equation (7). This diffusion behavior in this confined region cannot sustain a normal movement with a large time interval, and it is sufficient to calculate the diffusion coefficient within 20 ps. This greater placeholders of H<sub>2</sub>, ascribing to the lower blocking effect of N<sub>2</sub>, promote the faster movement of H<sub>2</sub>, as presented in Figure 7b. H<sub>2</sub> in three binary mixtures of H<sub>2</sub>/N<sub>2</sub>, H<sub>2</sub>/CH<sub>4</sub>, and H<sub>2</sub>/CO<sub>2</sub> exhibits the diffusion coefficients of  $0.57 \times 10^{-2}$ ,  $0.44 \times 10^{-2}$ , and  $0.33 \times 10^{-2}$  cm<sup>2</sup>/s, respectively. That is, the H<sub>2</sub> permeation is indeed impeded by the preferentially adsorbed CO<sub>2</sub> molecules. In other words, the GDY\_2.1Å can separate H<sub>2</sub> faster and more selectively from such a kind of binary mixture that the other species has a weak interaction toward GDY surfaces, such as H<sub>2</sub>/N<sub>2</sub>.

### 3.3. Surface Charge Effect

Two important mechanisms dominated the gas separation. This first one is the size sieving effect, which favors the permeation of small-sized molecules of H<sub>2</sub>. While beyond the size sieving effect, in the separation process of binary mixtures, the blocking effect greatly impedes H<sub>2</sub> permeation. This above understanding of the separation mechanism is beneficial to further guide the improvement of H<sub>2</sub> permeance particularly for the mixture of H<sub>2</sub>/CO<sub>2</sub> without sacrificing its selectivity. An effective way proposed here is to reduce the most severe blocking effect of CO<sub>2</sub> by surface charge modification. As depicted in the inset figure in Figure 8a, the positive and negative charges are uniformly imposed on the network of GDY\_2.1Å from  $\pm 0.00001$  to  $\pm 0.35$  e/atom, whereas the net charge of the whole membrane is zero. This CO<sub>2</sub> molecules still cannot cross the membrane regardless of surface charges. Compared to the pristine GDY membrane, the increased H<sub>2</sub> permeance of the binary mixture of H<sub>2</sub>/CO<sub>2</sub> was observed when surface charges are lower than  $\pm 0.1$  e/atom in Figure 8b. It can be up to  $2.84 \times 10^5$  GPU by imposing a tiny amount of surface charge of  $\pm 0.035$ – $0.050$  e/atom. This exceptionally



high permeance is several orders of magnitude greater than the existed experiments [40–42], which is ascribed to the ultimate pore size and atomic thickness of GDYs. This following decreasing trend in Figure 8b was ascribed to the surface overcharge, where the generated strong electrostatic repels not only CO<sub>2</sub> but also H<sub>2</sub> from approaching. Thus, achieving the perfect balance between these two mechanisms, a tiny amount of surface charges is qualified to maximize the H<sub>2</sub> permeance by reducing the blocking effect of strong interlaced molecules of CO<sub>2</sub>, meanwhile ensuring the placeholders of small-sized molecules of H<sub>2</sub> as well.

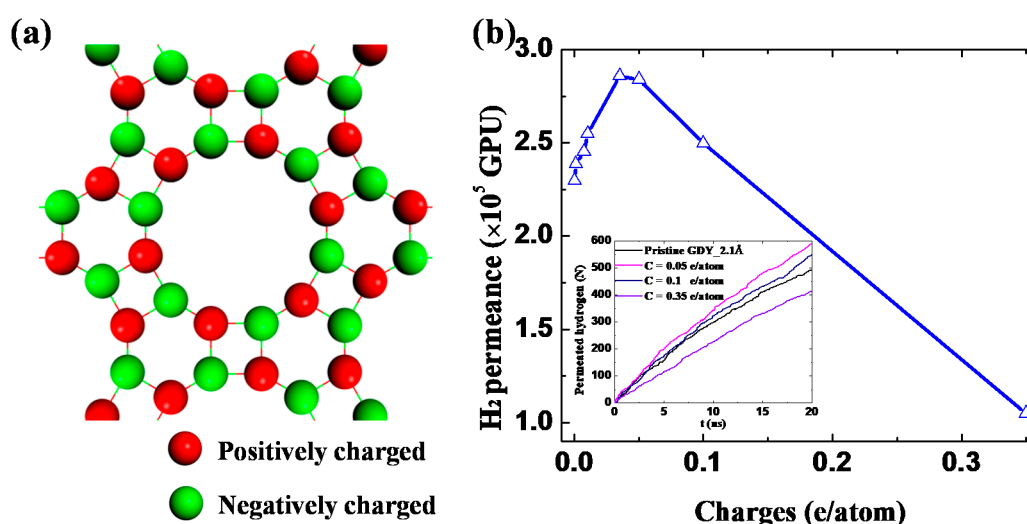


**Figure 8.** The effect of the surface charges on gas permeation. (a) The distribution of charges on the network of GDY\_2.1Å; (b) H<sub>2</sub> permeance of the binary mixture of H<sub>2</sub>/CO<sub>2</sub> as a function of surface charges. (Inset) The time evolution of permeated H<sub>2</sub> molecules through the charged GDYs.

#### 4. Conclusions

In summary, a multiscale study combining MD and DFT calculations was performed to investigate the gas permeation through carefully designed flexible GDY membranes with different pore structures and surface charges. Four single gases and three equimolar binary mixtures (H<sub>2</sub>/other gas) were simulated to study the selective gas permeation through GDYs. Approximately infinite selectivities of H<sub>2</sub> over N<sub>2</sub>, CO<sub>2</sub>, and CH<sub>4</sub> in GDY\_2.1Å membranes were demonstrated by DFT calculations. This underlying mechanism indicated that the blocking effect impeded H<sub>2</sub> permeation and the GDY\_2.1Å is prone to separate H<sub>2</sub> from such binary mixtures in which the other species has a weak gas–membrane interaction. Moreover, by imposing a tiny amount of surface charges, the H<sub>2</sub> permeance of the binary H<sub>2</sub>/CO<sub>2</sub> mixture was further enhanced up to  $2.84 \times 10^5$  GPU without sacrificing the selectivity. These excellent transport properties make the GDYs a promising candidate for efficient H<sub>2</sub> purification. Although the present work is a theoretical study, it is believable that the GDYs can be elaborately designed for realistic separations with the improvement of a well-controlled synthesis strategy.

**Supplementary Materials:** The following are available online at <http://www.mdpi.com/2077-0375/10/10/286/s1>, Video S1: The separation process of the binary mixture of H<sub>2</sub>/CO<sub>2</sub> through GDY\_2.1Å.

**Author Contributions:** Conceptualization, Q.L. and G.L.; Data curation, Q.L.; Formal analysis, Q.L.; Funding acquisition, G.L.; Investigation, Q.L.; Methodology, Q.L.; Resources, G.L.; Writing—original draft, Q.L.; Writing—review & editing, L.C. and G.L. All authors have read and agreed to the published version of the manuscript.

**Funding:** This work was financially supported by the National Natural Science Foundation of China (grant numbers 21922805, 21776125). We are grateful to the High-Performance Computing Center of Nanjing Tech University for supporting the computational resources.

**Conflicts of Interest:** The authors declare no conflict of interest.

## References

1. Corredor, J.; Perez-Pena, E.; Rivero, M.J.; Ortiz, I. Performance of rGO/TiO<sub>2</sub> photocatalytic membranes for hydrogen production. *Membranes* **2020**, *10*, 218. [[CrossRef](#)] [[PubMed](#)]
2. Staffell, I.; Scamman, D.; Velazquez Abad, A.; Balcombe, P.; Dodds, P.E.; Ekins, P.; Shah, N.; Ward, K.R. This role of hydrogen and fuel cells in the global energy system. *Energy Environ. Sci.* **2019**, *12*, 463–491. [[CrossRef](#)]
3. Parvasi, P.; Mohammad Jokar, S.; Basile, A.; Iulianelli, A. An on-board pure H<sub>2</sub> supply system based on a membrane reactor for a fuel cell vehicle: A theoretical study. *Membranes* **2020**, *10*, 159. [[CrossRef](#)]
4. Zhang, Y.; Xu, P.; Liang, S.; Liu, B.; Shuai, Y.; Li, B. Exergy analysis of hydrogen production from steam gasification of biomass: A review. *Int. J. Hydrog. Energy* **2019**, *44*, 14290–14302. [[CrossRef](#)]
5. Franchi, G.; Capocelli, M.; De Falco, M.; Piemonte, V.; Barba, D. Hydrogen production via steam reforming: A critical analysis of MR and RMM technologies. *Membranes* **2020**, *10*, 10. [[CrossRef](#)]
6. Zhang, Y.; Lee, W.H.; Seong, J.G.; Bae, J.Y.; Zhuang, Y.; Feng, S.; Wan, Y.; Lee, Y.M. Alicyclic segments upgrade hydrogen separation performance of intrinsically microporous polyimide membranes. *J. Membr. Sci.* **2020**, *611*, 118363. [[CrossRef](#)]
7. Ockwig, N.W.; Nenoff, T.M. Membranes for hydrogen separation. *Chem. Rev.* **2007**, *107*, 4078–4110. [[CrossRef](#)]
8. Casadei, R.; Giacinti Baschetti, M.; Yoo, M.J.; Park, H.B.; Giorgini, L. Pebax@2533/graphene oxide nanocomposite membranes for carbon capture. *Membranes* **2020**, *10*, 188. [[CrossRef](#)]
9. Castel, C.; Favre, E. Membrane separations and energy efficiency. *J. Membr. Sci.* **2018**, *548*, 345–357. [[CrossRef](#)]
10. Richard, W. Baker. Overview of membrane science and technology. In *Membrane Technology and Applications*; John Wiley & Sons, Ltd.: Chichester, UK, 2012; pp. 1–14.
11. Wang, S.; Yang, L.; He, G.; Shi, B.; Li, Y.; Wu, H.; Zhang, R.; Nunes, S.; Jiang, Z. Two-dimensional nanochannel membranes for molecular and ionic separations. *Chem. Soc. Rev.* **2020**, *49*, 1071–1089. [[CrossRef](#)]
12. Liu, G.; Jin, W.; Xu, N. Graphene-based membranes. *Chem. Soc. Rev.* **2015**, *44*, 5016–5030. [[CrossRef](#)] [[PubMed](#)]
13. Liu, G.; Jin, W.; Xu, N. Two-Dimensional-Material Membranes: A new family of high-performance separation membranes. *Angew. Chem.* **2016**, *55*, 13384–13397. [[CrossRef](#)] [[PubMed](#)]
14. Liu, Q.; Gupta, K.M.; Xu, Q.; Liu, G.; Jin, W. Gas permeation through double-layer graphene oxide membranes: The role of interlayer distance and pore offset. *Sep. Purif. Technol.* **2019**, *209*, 419–425. [[CrossRef](#)]
15. Liu, Q.; Liu, Y.; Liu, G. Simulation of cations separation through charged porous graphene membrane. *Chem. Phys. Lett.* **2020**, *753*, 137606. [[CrossRef](#)]
16. James, A.; John, C.; Owais, C.; Myakala, S.N.; Chandra Shekar, S.; Choudhuri, J.R.; Swathi, R.S. Graphynes: Indispensable nanoporous architectures in carbon flatland. *RSC Adv.* **2018**, *8*, 22998–23018. [[CrossRef](#)]
17. Gao, X.; Liu, H.; Wang, D.; Zhang, J. Graphdiyne: Synthesis, properties, and applications. *Chem. Soc. Rev.* **2019**, *48*, 908–936. [[CrossRef](#)]
18. Rezaee, P.; Naeij, H.R. Graphenylene-1 membrane: An excellent candidate for hydrogen purification and helium separation. *Carbon* **2020**, *157*, 779–787. [[CrossRef](#)]
19. Qiu, H.; Xue, M.; Shen, C.; Zhang, Z.; Guo, W. Graphynes for water desalination and gas separation. *Adv. Mater.* **2019**, *31*, e1803772. [[CrossRef](#)]
20. Mahdizadeh, S.J.; Goharshadi, E.K. Multicomponent gas separation and purification using advanced 2D carbonaceous nanomaterials. *RSC Adv.* **2020**, *10*, 24255–24264. [[CrossRef](#)]
21. Jiao, Y.; Du, A.; Hankel, M.; Zhu, Z.; Rudolph, V.; Smith, S.C. Graphdiyne: A versatile nanomaterial for electronics and hydrogen purification. *Chem. Commun.* **2011**, *47*, 11843–11845. [[CrossRef](#)]
22. Meng, Z.; Zhang, X.; Zhang, Y.; Gao, H.; Wang, Y.; Shi, Q.; Rao, D.; Liu, Y.; Deng, K.; Lu, R. Graphdiyne as a high-efficiency membrane for separating oxygen from harmful gases: A first-principles study. *ACS Appl. Mater. Interfaces* **2016**, *8*, 28166–28170. [[CrossRef](#)] [[PubMed](#)]
23. Zhao, L.; Sang, P.; Guo, S.; Liu, X.; Li, J.; Zhu, H.; Guo, W. Promising monolayer membranes for CO<sub>2</sub>/N<sub>2</sub>/CH<sub>4</sub> separation: Graphdinyne modified respectively with hydrogen, fluorine, and oxygen atoms. *Appl. Surf. Sci.* **2017**, *405*, 455–464. [[CrossRef](#)]

24. Apriliyanto, Y.B.; Lago, N.F.; Lombardi, A.; Evangelisti, S.; Bartolomei, M.; Leininger, T.; Pirani, F. Nanostructure selectivity for molecular adsorption and separation: The case of graphyne layers. *J. Phys. Chem. C* **2018**, *122*, 16195–16208. [[CrossRef](#)]
25. Sang, P.; Zhao, L.; Xu, J.; Shi, Z.; Guo, S.; Yu, Y.; Zhu, H.; Yan, Z.; Guo, W. Excellent membranes for hydrogen purification: Dumbbell-shaped porous  $\gamma$ -graphynes. *Int. J. Hydrog. Energy* **2017**, *42*, 5168–5176. [[CrossRef](#)]
26. Jiao, Y.; Du, A.; Smith, S.C.; Zhu, Z.; Qiao, S.Z. H<sub>2</sub> purification by functionalized graphdiyne—role of nitrogen doping. *J. Mater. Chem. A* **2015**, *3*, 6767–6771. [[CrossRef](#)]
27. Lei, G.; Liu, C.; Li, Q.; Xu, X. Graphyne nanostructure as a potential adsorbent for separation of H<sub>2</sub>S/CH<sub>4</sub> mixture: Combining grand canonical Monte Carlo simulations with ideal adsorbed solution theory. *Fuel* **2016**, *182*, 210–219. [[CrossRef](#)]
28. Bartolomei, M.; Giorgi, G. A novel nanoporous graphite based on graphynes: First-principles structure and carbon dioxide preferential physisorption. *ACS Appl. Mater. Interfaces* **2016**, *8*, 27996–28003. [[CrossRef](#)]
29. Zhang, H.; He, X.; Zhao, M.; Zhang, M.; Zhao, L.; Feng, X.; Luo, Y. Tunable hydrogen separation in sp-sp<sup>2</sup> hybridized carbon membranes: A first-principles prediction. *J. Phys. Chem. C* **2012**, *116*, 16634–16638. [[CrossRef](#)]
30. Bartolomei, M.; Carmona-Novillo, E.; Hernández, M.I.; Campos-Martínez, J.; Pirani, F.; Giorgi, G. Graphdiyne pores: “Ad Hoc” openings for helium separation applications. *J. Phys. Chem. C* **2014**, *118*, 29966–29972. [[CrossRef](#)]
31. Delley, B. An all-electron numerical method for solving the local density functional for polyatomic molecules. *J. Chem. Phys.* **1990**, *92*, 508–517. [[CrossRef](#)]
32. Lee, S.-M.; Kim, J.-H.; Ahn, J.-H. Graphene as a flexible electronic material: Mechanical limitations by defect formation and efforts to overcome. *Mater. Today* **2015**, *18*, 336–344. [[CrossRef](#)]
33. Zhou, K.; Xu, Z. Renormalization of ionic solvation shells in nanochannels. *ACS Appl. Mater. Interfaces* **2018**, *10*, 27801–27809. [[CrossRef](#)]
34. Wennberg, C.L.; Murtola, T.; Páll, S.; Abraham, M.J.; Hess, B.; Lindahl, E. Direct-space corrections enable fast and accurate Lorentz–Berthelot combination rule Lennard–Jones lattice summation. *J. Chem. Theory Comput.* **2015**, *11*, 5737–5746. [[CrossRef](#)] [[PubMed](#)]
35. Hess, B.; Kutzner, C.; van der Spoel, D.; Lindahl, E. GROMACS 4: Algorithms for highly efficient, load-balanced, and scalable molecular simulation. *J. Chem. Theory Comput.* **2008**, *4*, 435–447. [[CrossRef](#)] [[PubMed](#)]
36. Bussi, G.; Donadio, D.; Parrinello, M. Canonical sampling through velocity rescaling. *J. Chem. Phys.* **2007**, *126*, 014101. [[CrossRef](#)]
37. Essmann, U.; Perera, L.; Berkowitz, M.L.; Darden, T.; Lee, H.; Pedersen, L.G. A smooth particle mesh Ewald method. *J. Chem. Phys.* **1995**, *103*, 8577–8593. [[CrossRef](#)]
38. Xu, J.; Zhou, S.; Sang, P.; Li, J.; Zhao, L. Inorganic graphenylene as a promising novel boron nitrogen membrane for hydrogen purification: A computational study. *J. Mater. Sci.* **2017**, *52*, 10285–10293. [[CrossRef](#)]
39. Van Reis, R.; Zydney, A. Bioprocess membrane technology. *J. Membr. Sci.* **2007**, *297*, 16–50. [[CrossRef](#)]
40. Omidvar, M.; Nguyen, H.; Liang, H.; Doherty, C.M.; Hill, A.J.; Stafford, C.M.; Feng, X.; Swihart, M.T.; Lin, H. Unexpectedly strong size-sieving ability in carbonized polybenzimidazole for membrane H<sub>2</sub>/CO<sub>2</sub> separation. *ACS Appl. Mater. Interfaces* **2019**, *11*, 47365–47372. [[CrossRef](#)]
41. Sun, Y.; Song, C.; Guo, X.; Liu, Y. Concurrent Manipulation of out-of-plane and regional in-plane orientations of NH<sub>2</sub>-UiO-66 membranes with significantly reduced anisotropic grain boundary and superior H<sub>2</sub>/CO<sub>2</sub> separation performance. *ACS Appl. Mater. Interfaces* **2020**, *12*, 4494–4500. [[CrossRef](#)]
42. Robeson, L.M. This upper bound revisited. *J. Membr. Sci.* **2008**, *320*, 390–400. [[CrossRef](#)]

**Publisher’s Note:** MDPI stays neutral with regard to jurisdictional claims in published maps and institutional affiliations.



© 2020 by the authors. Licensee MDPI, Basel, Switzerland. This article is an open access article distributed under the terms and conditions of the Creative Commons Attribution (CC BY) license (<http://creativecommons.org/licenses/by/4.0/>).